IEEE Access
Multidisciplinary | Rapid Review | Open Access Journal

Received June 24, 2019, accepted July 13, 2019, date of publication July 24, 2019, date of current version August 9, 2019.

Digital Object Identifier 10.1109/ACCESS.2019.2930747

Differential Permittivity Sensor Using Microstrip Terminated Cross-Shaped Resonator Structure for Material Characterization

CHI-HOU CHIO[1], (Student Member, IEEE), CHENG TENG[1], (Student Member, IEEE), KAM-WENG TAM[1], (Senior Member, IEEE), WAI-WA CHOI[1], (Senior Member, IEEE), PEDRO CHEONG[1,2], (Member, IEEE), AND SUT-KAM HO[1]

[1]Department of Electrical and Computer Engineering, University of Macau, Macau SAR 999078, China
[2]Poly-Grames Research Center and Center for Radiofrequency Electronics Research of Quebec (CREER), Department of Electrical Engineering, Ecole Polytechnique de Montreal, Montreal, QC H3T 1J4, Canada

Corresponding author: Chi-Hou Chio (yb57422@umac.mo)

This work was supported in part by the Macao Science and Technology Development Fund under Grant FDCT 014/2015/AMJ, and in part by the University of Macau Research Projects under Grant MYRG 2018-00076-FST.

ABSTRACT A differential planar microwave resonator permittivity sensor for material characterization is proposed in this paper. The sensor is based on asymmetric terminated cross-shaped resonator (TCSR) to provide multi-band notch frequency characteristics, allowing permittivity measurement of a small dielectric material under test (MUT) with a single resonator. Differential sensing is robust against varying ambient factors that cause frequency variations in the measurements. The dielectric properties of the MUT can be measured from the difference in notch frequencies with the reference material. To illustrate the technique, a tri-band sensor is prototyped using the proposed resonator configuration to measure the permittivity of both solid and liquid samples. The empirical equations for the determination of the MUT permittivity in relation to the notch frequencies have been derived. The sensor operates at 0.97, 1.69, and 2.91 GHz with an average sensitivity of 1.18, 4.45, and 1.22 MHz, respectively. The measured results are in a good agreement with the theoretical analysis.

INDEX TERMS Microwave sensors, material characterization, permittivity sensors, differential sensors, cross-shaped resonator, microstrip technology.

I. INTRODUCTION

Microwave sensors come in many forms and have numerous applications in the industry [1]. Several applications include material characterization [2]–[22], velocity and displacement detection [23]–[25], thickness sensing [26], strain detection [27], and skin sensing [28]. Microwave frequency is defined as the frequency between 300 MHz to 300 GHz, which has wavelengths of about 1 mm to 1 m. This frequency region is commonly used in numerous communication systems such as mobile communication system, Wi-Fi system, satellite system, radar system, and terrestrial TV broadcasting system.

Microwave sensors rely on the interactions between microwave and the materials as a mean for sensing. These interactions include transmission, reflection, refraction, scattering, absorption, and the resulting changes in the signal magnitude, velocity, phase, and sometimes polarization. The behavior of these responses depends on the properties of the material that microwave interacts with, which can be characterized by permittivity ε, and permeability μ. Microwave sensors offer many advantages include the possibility of fast, contactless sensing. Moreover, because microwave can propagate into many materials, sensing within a material is possible. Microwave sensors provide a stable and consistent measurement and are insensitive to the ambient conditions. One type of microwave sensor is the resonator-based sensor. Resonator is a guided wave structure, typically a transmission line (e.g., coaxial cable, strip-line, microstrip, slot-line, coplanar-waveguide, etc.) with discontinuities at the boundaries that allow waves to reflect and forms constructive interference at the resonant frequency. The frequency of resonance

The associate editor coordinating the review of this manuscript and approving it for publication was Feng Lin.

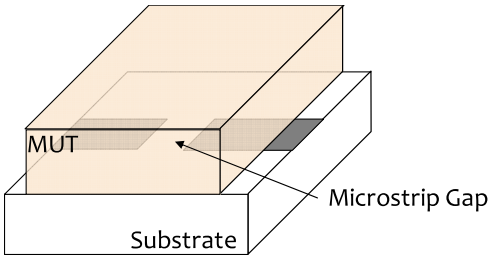

FIGURE 1. Illustration of MUT on top of a microstrip gap of a permittivity sensor.

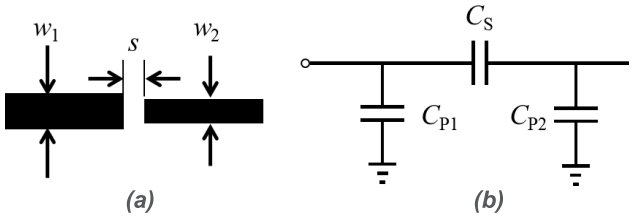

FIGURE 2. Microstrop gap. (a) Top view of a physical model. (b) Lumped circuit model.

is influenced by dielectric around the resonator, and it can, therefore, be used for determining the permittivity of a material.

An advantage of microwave resonator sensors over the non-resonator microwave sensor is its stability because the resonant frequency of the resonator is determined by the physical dimensions. Resonator sensor can be implemented with the resonator surrounded by the material under test (MUT), which allows the response to be sensitive to the losses of the MUT and allows easier permittivity calculation. Other implementations exposed part of the resonator to the MUT, which can be used for more lossy MUT, and requires less sample. However, establishing the theoretical relationship between the measured response and MUT permittivity can be difficult and will require calibration or curve fitting.

Microstrip gap, as illustrated in FIGURE 1, is often used in the dielectric measurement of material in small quantities, be it micro-fluidic sensing [2], [3], [8], [18], [29], thin films [17], or other solid materials. A microstrip gap forms a capacitive region between the two physically separated conductors and can be modeled by a series coupling capacitor C_s that is connected to shunt capacitors C_{P1} and C_{P2} on both ends, as shown in FIGURE 2. Modeling for the capacitance of the microstrip gap as a function of the dielectric constant of the PCB and the dimensions can be found in [30]–[33]. The model can be simplified to use only C_s to represent the microstrip gap. The relationship between C_s and permittivity of the MUT ε_{rMUT} can, therefore, be approximated by a linear relationship [2], [4] as follows

$$C_s = C_{s0} + \varepsilon_{rMUT} C_{sMUT} \tag{1}$$

where C_{s0} represents the capacitance from the dielectric substrate and the surrounding space, excluding the MUT placement region. The term $\varepsilon_{rMUT}C_{sMUT}$ represents the capacitance contribution due to the placement of the MUT, in which C_{sMUT} represents the capacitance contribution without MUT loading. The frequency sensitivity of the sensor to the MUT is related to the area of which the sensor interacts with the MUT. Larger MUT coverage will increase the sensitivity at the expense of requiring a larger amount of sample.

Differential sensing with microwave resonators has been gaining attention lately for their ability to reduce the effects of environmental factors such as temperature and humidity to the measurement. This type of sensor determines the permittivity of the MUT by using the difference in resonant frequencies between the MUT and a reference material, where the reference can be a material similar to the MUT or being left vacant. Two independent sensors of the same kind can be used to form a differential sensor. When a differential sensor is used as a single material sensor, MUT will be arranged on one end of the sensor, and the permittivity can be determined from the difference in resonant frequency Δf_z. When used as a comparator, two materials will be placed on each end of the sensor to determine if the materials have different permittivity. One of the materials may have known characteristics to serve as a reference material like how dial indicator and gage blocks are used to conduct length measurements. However, with two sensors require two sets of input/output for measurement, making the measurement process more difficult. There are exceptions, for example, in [7], differential sensor formed by two identical, but independent single-port sensors are used to measure the difference in resonant frequency with the reflection coefficient.

Differential resonator sensors based on frequency splitting have been proposed that allow differential measurement with one pair of input and output port [6], [9], [10], [14], [15], [20]–[22]. This type of sensor relies on the disruption of resonator symmetry to generate two notch frequencies. When the resonators are symmetrically loaded with the same MUT, only one notch frequency will appear. However, when the symmetry is broken due to asymmetric MUT loading, the notch frequency will be split into two. The differential frequency is determined by the level of asymmetry of the loadings; hence, differential sensor is robust against the variations of the common-mode ambient factors. The advantages of single-ended two port sensors have over four port designs include simplified measurement steps and the requirement for measuring devices. There are several implementations of frequency splitting based differential sensor. Using microstrip splitter/combiner architecture, differential sensors have been proposed with a pair of transmission line in parallel that is being loaded with split ring resonators (SRR) [14], complementary split ring resonator (CSRR) [6] or step impedance resonators (SIR) [15]. In [10], SIR with half-wavelength separation are loaded on a transmission line to reduce inter-resonator coupling and improve sensitivity. In [21], [22], a pair of SRR/CSRR is loaded on a transmission line in parallel to create a differential sensor. In [9], a dual-mode resonator was proposed to provide differential sensing

with a single SRR, with the differential sensing implemented using an algorithm.

Typical resonator sensors operate at a single frequency band, and therefore can only characterize MUT at a single frequency range. For dispersive samples such as aqueous solutions, multi-band sensing is beneficial because the dielectric properties of these materials are frequency dependent. There are many implementations of multi-band sensors using multiple resonators. In [4], a quad-band resonator sensor is realized by loading four CSRR to a transmission line. In [16], a dual-band permittivity and thickness sensor is implemented using a single-compound CSRR that is formed by nesting two CSRR to generate two distinct resonance current lengths. For single-band differential resonator sensors, except for the dual-mode resonator approach in [9], are realized using two resonators in combination. For multi-band differential sensors, implementations by cascading multiple individual differential sensors have been reported [15], [20]. A disadvantage with the multi-resonator setup is that each resonator requires the placement of a sample for the sensor to operate, which makes multi-band sensing cumbersome for the scenario where the size of the sample is small. Also, each additional resonator will increase the size of the overall sensor. Currently, there is a lack of a single resonator implementation of a multi-band differential resonator sensor.

In the realm of planar microstrip filters, multiple-mode resonator (MMR) [34], [35] and defected ground structure (DGS) [36] are widely used. A novel MMR called the terminated cross-shaped resonator (TCSR) has been researched by many to realize bandstop filters with controllable notch bands [37], [38] . The transmission poles and zeroes for symmetric TCSR with different terminations have been studied extensively. The capacitor loaded TCSR, for instance, allows the generation of multiple in-band transmission zeros with notch frequencies f_z controllable by changing the capacitance, and this property can be used for material sensing. In this paper, a tri-band differential microwave sensor based on TCSR technique, useful for characterization of small liquid and solid sample, is proposed. This design uses a single resonator to achieve multi-band differential sensing, which has the advantage of compact size and only requires a single small sample to operate. To the best of our knowledge, this is the first microwave resonator sensor that can provide multi-band and differential sensing functionality simultaneously using a single resonator.

II. ANALYSIS OF TERMINATED CROSS-SHAPED RESONATOR WITH ASYMMETRIC CAPACITIVE LOADING

The proposed TCSR structure is shown in FIGURE 3. The parameters θ_n and $Z_n (n = 1, 2, 3)$ denote the electrical lengths and characteristic impedances of these transmission lines, respectively. The TCSR is formed by a transmission line (Z_1, θ_1) loaded with an open stub (Z_3, θ_3), and two transmission lines (Z_{2a}, θ_{2a}) and (Z_{2b}, θ_{2b}) loaded with capacitive termination of C_{L2a} and C_{L2b} respectively. The capacitors

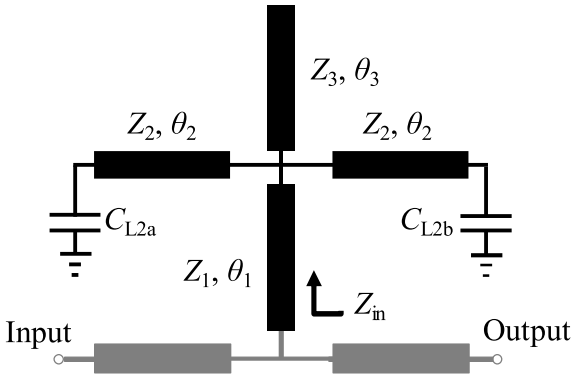

FIGURE 3. Schematic of the proposed TCSR (in black) with open and capacitive terminations.

can be replaced by microstrip gaps using (1) as described in the previous section to represent the placement of MUT. The TCSR is loaded to a transmission line to provide the input and output to the circuit.

The input impedance Z_{in} of the resonators can be expressed as

$$Z_{in} = Z_1 \frac{Z_{C1} + jZ_1 \tan\theta_1}{Z_1 + jZ_{C1} \tan\theta_1} \tag{2a}$$

where

$$Z_{C1} = \frac{Z_{C2a} Z_{C2b} Z_3}{Z_3(Z_{C2a} + Z_{C2b}) + jZ_{C2a} Z_{C2b} \tan\theta_3} \tag{2b}$$

$$Z_{C2a} = jZ_{2a} \frac{\omega C_{L2a} Z_{2a} \tan\theta_{2a} - 1}{\omega C_{L2a} Z_{2a} + \tan\theta_{2a}} \tag{2c}$$

$$Z_{C2b} = jZ_{2b} \frac{\omega C_{L2b} Z_{2b} \tan\theta_{2b} - 1}{\omega C_{L2b} Z_{2b} + \tan\theta_{2b}} \tag{2d}$$

To simplify the analysis, we assume that all transmission lines of the resonator share the same characteristic impedance $Z_2 = Z_{2a} = Z_{2b} = Z_3 = 50\Omega$ and electrical length $\theta = \theta_{2a} = \theta_{2a} = \theta_3 = \pi/2$ at f_0. The frequency f_0 will be set as 2 GHz from here on for the convenience of analysis. When $C_{L2a} = C_{L2b} = 0$, there are two transmission zeros, f_{z1} and f_{z4}, symmetrically located below and above f_0 respectively that are generated by the transmission line portion of the resonator. The frequencies of transmissions zero f_{z1} and f_{z4} can be expressed as

$$f_{z1} = \frac{2f_0}{\pi} \tan^{-1}\left[\sqrt{\frac{Z_2 Z_3}{Z_1 (Z_2 + 2Z_3)}}\right] \tag{3a}$$

$$f_{z4} = \frac{2f_0}{\pi} \tan^{-1}\left[-\sqrt{\frac{Z_2 Z_3}{Z_1 (Z_2 + 2Z_3)}}\right] \tag{3b}$$

A. SYMMETRIC CHARACTERISTICS

When $C_{L2b} = C_{L2b} = C_L > 0$, an additional transmission zero f_{z3} will be generated at a frequency between f_{z1} and f_0, which can be expressed as

$$f_{z3} = \frac{2f_0}{\pi} \tan^{-1}\left[\frac{1}{3C_L Z_1^2 Z_2 \omega}\left(3Z_1^2 + C_A + \frac{\Delta_0}{C_A}\right)\right] \tag{4a}$$

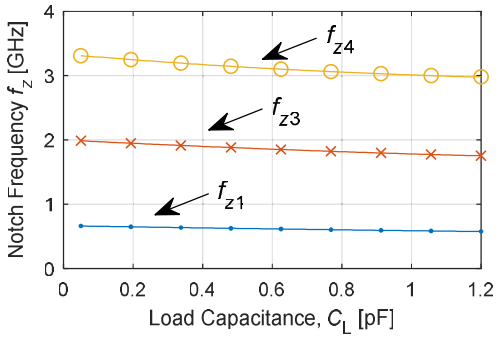

FIGURE 4. Notch frequency vs different C_L =$_{L2a}$= C_{L2b}, for $Z_1 = Z_2 = Z_3 = 50\Omega$.

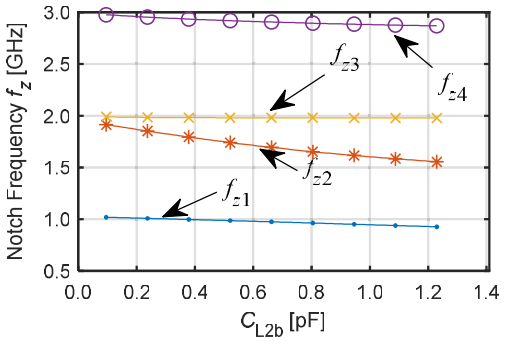

FIGURE 5. Notch band frequencies vs C_{L2b}, where $C_{L2a} = 0.05$ pF to represent an unlocaded microstrip gap, $Z_1 = Z_2 = Z_3 = 50\ \Omega$.

where

$$C_A = \sqrt[3]{\frac{\Delta_1 + \sqrt{\Delta_1^2 - 4\Delta_0^2}}{2}} \tag{4b}$$

$$\Delta_0 = 9Z_1^4 + 3C_L^2 Z_1^3 Z_2^2 \omega^2 (2Z_1 + Z_2) \tag{4c}$$

$$\Delta_1 = 54Z_1^6 \left(C_L^2 Z_2^2 \omega^2 + 1\right) \tag{4d}$$

The notch frequencies f_{z1}, f_{z3}, and f_{z4} are lowered as C_L increases, as shown in FIGURE 4.

B. ASYMMETRIC CHARACTERISTICS

When $C_{L2a} \neq C_{L3b}$, the symmetry of the resonator is disrupted and if both values are non-zero, an additional transmission zero f_{z2} would be generated. Equation (5) provides a good representation to f_{z2} when $C_{L2b} > 2C_{L2a}$.

$$f_{z2} = \frac{2f_0}{\pi} \tan^{-1}\left[\frac{1}{2C_{L2new}Z_1^2 Z_2 \omega}\left(3Z_1^2 + C_B + \frac{\Delta_2}{C_B}\right)\right] \tag{5a}$$

where

$$C_B = \sqrt[3]{\frac{\Delta_3 + \sqrt{\Delta_3^2 - 4\Delta_2^2}}{2}} \tag{5b}$$

$$\Delta_2 = 9Z_1^4 + 6C_{L2new}^2 Z_1^3 Z_2^2 \omega^2 (Z_1 + Z_2) \tag{5c}$$

$$\Delta_3 = 54Z_1^5 \left(Z_2^2 \omega^2 C_{L2new}^2 (Z_1 - Z_2) + Z_1\right) \tag{5d}$$

$$C_{L2new} = C_{L2b} + C_{L2a}/3 \tag{5e}$$

According to the analysis above, the transmission zeros f_{z1} and f_{z4} are generated by the CSR and exist without the capacitive loadings. The notch frequency f_{z3} is generated by the symmetric capacitance terminations, while f_{z2} is formed due to the asymmetry of the capacitive loadings.

C. ANALYSIS OF TCSR NOTCH FREQUENCY CHARACTERISTICS

FIGURE. 5 shows the notch frequencies of the TCSR with asymmetric capacitive loading. We define $\Delta f_{z31} = |f_{z3} - f_{z1}|$, $\Delta f_{z34} = |f_{z4} - f_{z3}|$, $\Delta f_{z23} = |f_{z3} - f_{z2}|$ and $\Delta C_{L2} = |C_{L2a} - C_{L2b}|$. When C_{L2b} increases and other parameters remain unchanged, the notch frequencies f_{z1}, f_{z2}, f_{z4} would be lowered, while f_{z3} would stay unchanged compared to the other notches. The f_{z2} and f_{z3} is the frequency splitting pair due to asymmetric loading, and their difference Δf_{z23} can provide differential sensing information when the TCSR is used in a permittivity sensor. Also, although f_{z1} and f_{z4} are formed by the CSR intrinsically, the behavior of the frequency difference Δf_{z31} and Δf_{z34} exhibit traits of behaviors that we expect from differential resonator sensors. From FIGURE 4, we can observe that when the TCSR is under symmetric load C_L, for a small variation in C_L, Δf_{z31}, and Δf_{z34} remain mostly unchanged. This provides a common-mode resistance to ambient environment interference. On the other hand, the frequency difference Δf_{z31} and Δf_{z34} are sensitive to the change in the asymmetric capacitive loading ΔC_{L2}, as shown in FIGURE. 5. Therefore, the proposed TCSR can generate four notches and can provide differential sensing capability for three bands with $\Delta f_{z31}\Delta f_{z23}$ and Δf_{z34}. However, since the reference frequency is at f_{z3}, Δf_{z31} and Δf_{z34} does not give optimum permittivity results for dispersive materials but should be adequate for dielectric characterization with empirical equations. For the configuration in FIGURE. 5, the TCSR can be used as a sensor with frequency bands located around 1 GHz, 1.7 GHz and 2.9 GHz, with Δf_{z23} being the most sensitivity to change in the difference in the capacitance ΔC_{L2}.

The line impedance Z_1 provides independent control over the outer notch frequency of the resonator, f_{z1}, and f_{z4}. For fixed $Z = Z_2 = Z_3$, when the Z/Z_1 ratio increases, the f_{z1} and f_{z4} move closer to f_0 without affecting f_{z2} and f_{z3}, as shown in FIGURE 6 (a). With this control parameter, we can assign the starting location for f_{z1} and f_{z4}. The frequency f_{z1} to f_{z4}, on the other hand, decrease as θ_2 increases, as shown in FIGURE 6 (b). Therefore, by changing Z/Z_1, θ, and θ_2/θ, the relative locations of f_{z1} to f_{z4} can be adjusted.

III. IMPLEMENTATION OF TCSR BASED MICROWAVE SENSOR

To demonstrate the proposed method, the sensor is designed on PCB board RO4003C with substrate permittivity

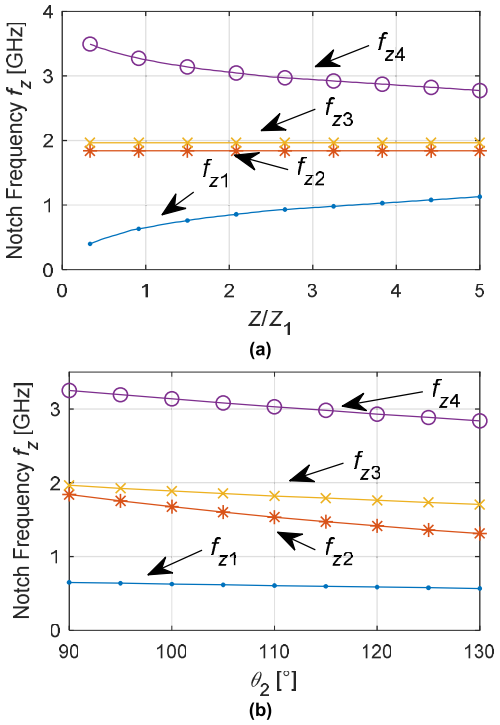

FIGURE 6. Notch frequencies for asymmetric termination, where $C_{L2a} = 0.1$ pF and $C_{L2b} = 0.3$ pF, vs (a) Z_1, and (b) θ_2.

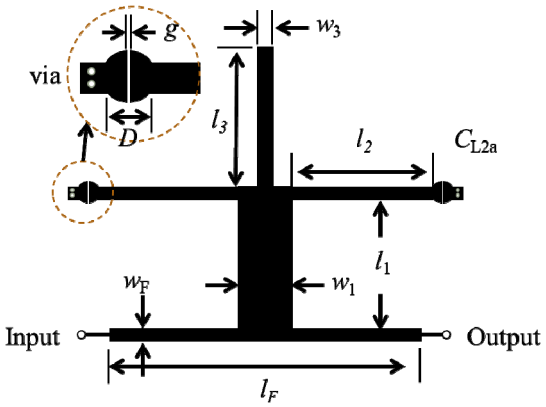

FIGURE 7. Layout of differential permittivity sensor using microstrip cross-shaped resonator structure.

$\varepsilon_r = 3.38$ and height $h = 0.812$ mm. The layout of the design is shown in FIGURE 7. The capacitors are replaced with microstrip gaps, and each of them is implemented using a circle with a gap in the middle to allow larger MUT placement area. The dimensions of the sensor are as follow: $l_1 = 23.1$ mm, $l_2 = 20.6$ mm, $l_3 = 20.8$ mm, $l_F = 29$ mm, $w_1 = w_2 = w_3 = w_F = 1.72$ mm, diameter of the microstrip gap $D = 2.5$ mm with gap width $g = 0.2$ mm. The overall size of the sensor is 54 mm × 66 mm ($0.60\lambda_g \times 0.73\lambda_g$ at f_0). Simulation of the sensor is conducted using Ansys HFSS. FIGURE 8 shows the simulation result for the proposed sensor with different MUT loading on one microstrip gap and vacant on the other side, illustrating the effect of

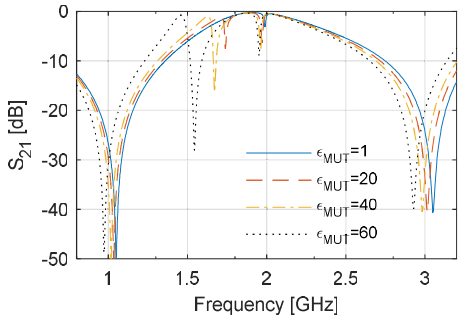

FIGURE 8. Simulation result of the TCSR based differential permittivity sensor under different dielectric load.

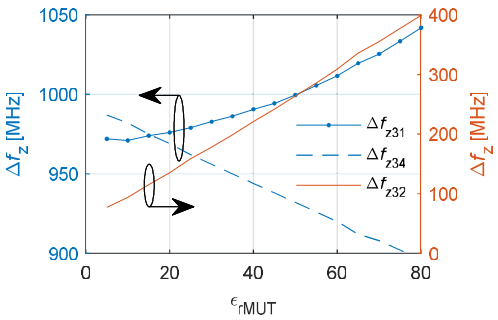

FIGURE 9. Δf_z of different bands vs ε_{rMUT}.

frequency splitting on f_{z2} and f_{z3} due to asymmetric loading of microstrip gap as well as f_{z3} and f_{z4}.

Analysis of the sensor Δf_z is performed by assuming that the microstrip gap on one side is unloaded ($\varepsilon_{rMUTa} = 1$) and loaded with various the cylindrical MUT on the other end (ε_{rMUTb}) with a diameter of 2.5 mm and height $h_{MUT} = 0.60$ mm. The MUT dimension is chosen for illustration, and Δf_z varies with different MUT sizes. The relationship between the Δf_z and ε_{rMUT} for different frequency band are obtained from simulations is shown in FIGURE 9.

The sensor is prototyped using the LPKF C100 milling machine, and measurement is conducted using Anritsu MS4624D vector network analyzer (VNA) to verify the design. Results from different MUT, a solid sample, and a liquid sample are obtained by loading the MUT on one side of the sensor. The solid sample is a piece of RO4003C substrate with a thickness of 1.524 mm, a length of 1.1 mm and a width of 0.2 mm, with the length of dielectric aligned to the top of the microstrip gap in parallel with the gap. For the liquid sample, a water droplet of 8 μL in volume is applied precisely using a micro-pipette. The results of the measurement in comparison with the EM simulation is illustrated in FIGURE 10 and FIGURE 11. The figures show a good overall match between the two and the deviation can be attributed to fabrication tolerance. The sensor can also measure liquid droplets with relatively high surface tension such as sucrose solution and saline solution but is not demonstrated here.

A comparison of the average sensitivity S_{av} of different microwave resonator sensors that accept small MUT is shown

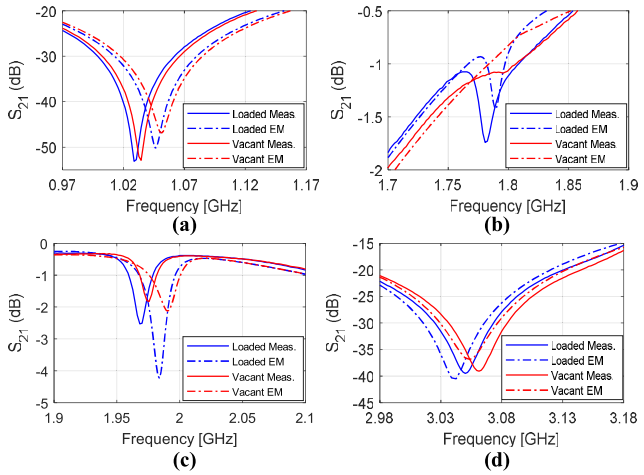

FIGURE 10. Measured and simulated result of TCSR based differential permittivity sensor loaded with RO4003C with $h_{MUT} = 1.542$ mm and vacant without loading. (a) f_{z1}, (b) f_{z2}, (c) f_{z3}, and (d) f_{z4}.

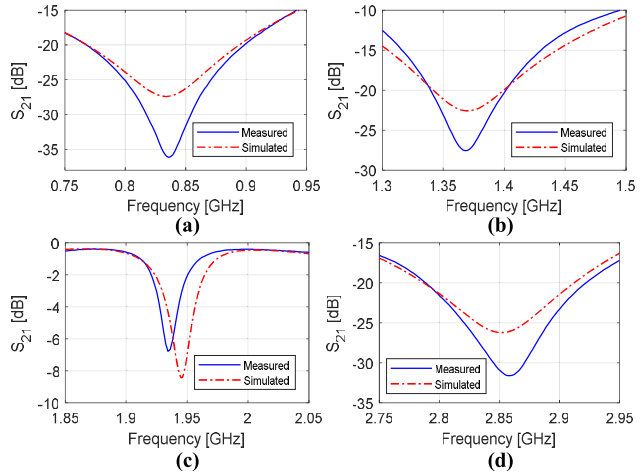

FIGURE 11. Measured and simulated result of TCSR based differential permittivity sensor loaded with distilled water. (a) f_{z1}, (b) f_{z2}, (c) f_{z3}, and (d) f_{z4}.

TABLE 1. Comparison of the Sensitivity Different Microwave Sensors With Small MUT.

Ref.	f_c (GHz)	S_{av} (MHz)	$S_{av,f}$ (%)
[2]	1.9	1.53	0.081
[11]	0.9	1.8	0.186
[12]	2.5	8	0.320
[13]	3.5	9.16	0.261
[14]	0.87	0.79	0.0091
[19]	2	4.76	0.238
[17]	2.02/2.35/2.69/3.03	1.25/1.38/2.13/6.37	0.062/0.059/0.079/0.211
T.W.	**0.97/1.69/2.91**	**1.18/4.45/1.22**	**0.121/0.263/0.042**

in Table I. The sensitivity is defined as follows

$$|S| = \frac{\partial \Delta f_z}{\partial \Delta \varepsilon_r} \tag{6}$$

where the $\Delta\varepsilon_r = |\varepsilon_{rMUT} - \varepsilon_{rREF}|$ is the difference in relative permittivity between the MUT and the reference material, $\varepsilon_{rREF} = 1$ in this case. The average sensitivity S_{av} takes

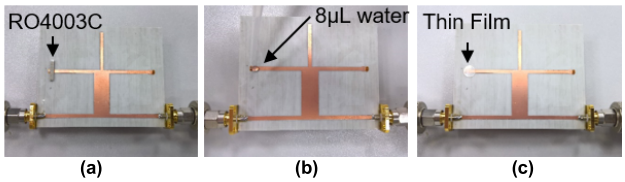

FIGURE 12. Photo of the prototyped sensor with different MUT. (a) RO4003C, (b) 8 μL distilled water, and (c) Thin-film.

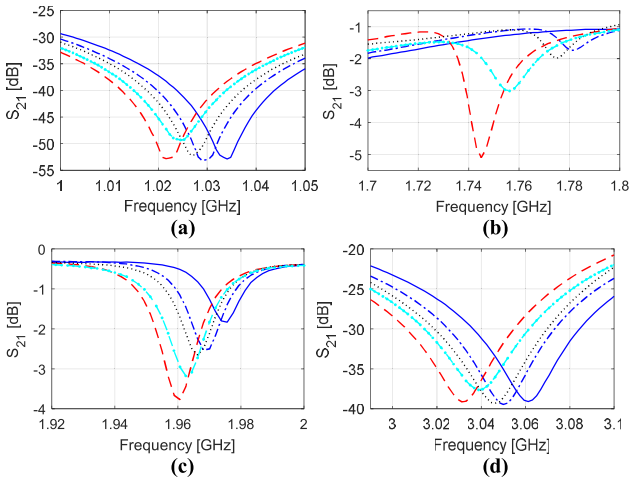

FIGURE 13. Measured result of TCSR based differential permittivity sensor under different dielectric load, Vacant (———), MUT 1 (—·—·—), MUT 2 (— — —), MUT 3 (·····) MUT 4 (— ·· —). (a) f_{z1}, (b) f_{z2}, (c) f_{z3}, and (d) f_{z4}.

the mean of $|S|$ over the detection range, and $S_{av,f}$ is S_{av} divided by the center frequency f_c. For the proposed design, the three bands operate at 0.97, 1.69 and 2.91 GHz, and have S_{av} of 1.18, 4.45 and 1.22 MHz, respectively. As shown in the table, the $S_{av,f}$ of the proposed sensor is comparable with other planar microwave resonator sensors that accept small MUT.

Several solid samples are tested on this differential sensor to illustrate that it can be used for measuring different MUT. MUT 1 is RO4003 with a thickness of 1.524 mm mentioned earlier. MUT 2 is Roger RO3210, and MUT 3 is FR4 with permittivity of 10.2 and 4.6 respectively and have the same dimension as MUT 1. MUT 4 is indium tin oxide (ITO) coated thin film with a thickness of 0.13 mm and a diameter of 5 mm, included to demonstrate that this sensor can detect thin film samples. The photo of the prototyped sensor, along with MUT placement, is shown in FIGURE 12. The result of the measurements is shown in FIGURE 13. While f_{z3} stays relatively constant for different MUT, it still varies from 1.9756 GHz to 1.9606 GHz for the materials listed, but it approaches a constant value as ε_{rMUT} increases.

To demonstrate the functionality of the sensor for permittivity sensing, the three MUT with known ε_{rMUT}, MUT 1 to MUT 3 are used for establishing an empirical model from simulation and measurement results to associate the permittivity ε_{rMUT} and the Δf_z for each frequency band.

TABLE 2. Measured Frequency Responses and Permittivity of Different MUT.

Parameter	Vacant	MUT 1	MUT 2	MUT 3
Material	-	RO4003C	RO3210	FR4
f_{z1} [a]	1.0344	1.0288	1.0208	1.0269
f_{z2} [a]	-	1.7806	1.7450	1.7750
f_{z3} [a]	1.9756	1.9681	1.9606	1.9663
f_{z4} [a]	3.0612	3.0500	3.0313	3.0463
Δf_{z31} [b]	941.25	939.375	939.775	939.450
Δf_{z32} [b]	-	187.5	215.625	191.250
Δf_{z34} [b]	1085.625	1081.875	1070.625	1080.0
$\lvert S_{21}\rvert$ [c] @ f_{z1}	-52.8754	-53.146	-52.8339	-52.2536
$\lvert S_{21}\rvert$ [c] @ f_{z2}	-1.9499	-1.7414	-5.0988	-1.9909
$\lvert S_{21}\rvert$ [c] @ f_{z3}	-	-2.5312	-3.7732	-2.6585
$\lvert S_{21}\rvert$ [c] @ f_{z4}	-39.0942	-39.471	-39.1445	-39.3164
ε_{rMUT} (meas.)	-	3.36	10.32	4.50
ε_{rMUT} (given)	-	3.38±0.05[d]	10.2±0.5[d]	4.4-4.6[e]

[a] in GHz, [b] in MHz, [c] in dB, [d] datasheet value, [e] typical value

The equations are as follows

$$\varepsilon_{rMUT31} = 17050\Delta f_{z31} - 16013 \quad (7a)$$

$$\varepsilon_{rMUT32} = -1828.2\Delta f_{z32}{}^2 + 986.27\Delta f_{z32} - 117.29 \quad (7b)$$

$$\varepsilon_{rMUT34} = -7332.1\Delta f_{z34}{}^2 + 15150\Delta f_{z34} - 7805.16 \quad (7c)$$

where the Δf_z are in GHz, for ε_{rMUT} between 3 to 11. Since the dimensions of the MUT have an influence on the resonant frequencies, this set of equations is only applicable to MUT of the same physical size. The empirical model for water droplet and thin film samples can be established separately. Using (7) and the measured Δf_z, the ε_{rMUT31}, ε_{rMUT32}, and ε_{rMUT34} are 3.34, 3.36, 3.36 for MUT 1, 10.16, 10.37, 10.48 for MUT 2, and 4.51, 4.46, 4.68 for MUT 3 respectively . The overall ε_{rMUT} of MUT 1 to MUT 3 are computed by using weighted sum with the $S_{av,f}$ of each band as the coefficients. The results are listed in TABLE II and show a good agreement between the measured permittivity and the known values from the datasheets.

IV. CONCLUSION

A novel tri-band planar microwave resonator sensor based on asymmetric TCSR with differential sensing capability is proposed for material characterization. A prototype operating at 0.97, 1.69 and 2.91 GHz with a dimension of 54 mm × 66 mm is designed, fabricate, and tested. The principle of this sensor is based on the capacitance change of the TCSR terminations that is generated by the placement of MUT to cause variations of multiple notch frequencies. This approach uses a single resonator to provide multi-band and differential sensing functionalities simultaneously, thus allowing a compact sensor design that can accept small solid or liquid MUT.

REFERENCES

[1] E. Nyfors, "Industrial microwave sensors—A review," *Subsurface Sens. Technol. Appl.*, vol. 1, no. 1, pp. 23–43, Jan. 2000.
[2] W. Withayachumnankul, K. Jaruwongrungsee, A. Tuantranont, C. Fumeaux, and D. Abbott, "Metamaterial-based microfluidic sensor for dielectric characterization," *Sens. Actuators A, Phys.*, vol. 189, pp. 233–237, Jan. 2013.
[3] D. J. Rowe, S. Al-Malki, A. A. Abduljabar, A. Porch, D. A. Barrow, and C. J. Allender, "Improved split-ring resonator for microfluidic sensing," *IEEE Trans. Microw. Theory Techn.*, vol. 62, no. 3, pp. 689–699, Mar. 2014.
[4] M. A. H. Ansari, A. K. Jha, Z. Akhter, and M. J. Akhtar, "Multi-band RF planar sensor using complementary split ring resonator for testing of dielectric materials," *IEEE Sensors J.*, vol. 18, no. 16, pp. 6596–6606, Apr. 2018.
[5] M. S. Boybay and O. M. Ramahi, "Material characterization using complementary split-ring resonators," *IEEE Trans. Instrum. Meas.*, vol. 61, no. 11, pp. 3039–3046, Nov. 2012.
[6] L. Su, J. Mata-Contreras, P. Vélez, and F. Martín, "Splitter/combiner microstrip sections loaded with pairs of complementary split ring resonators (CSRRs): Modeling and optimization for differential sensing applications," *IEEE Trans. Microw. Theory Techn.*, vol. 64, no. 12, pp. 4362–4370, Dec. 2016.
[7] A. Ebrahimi, J. Scott, and K. Ghorbani, "Transmission lines terminated with LC resonators for differential permittivity sensing," *IEEE Microw. Wireless Compon. Lett.*, vol. 28, no. 12, pp. 1149–1151, Dec. 2018.
[8] Y. Cui, Y. He, and P. Wang, "A quadrature-based tunable radio-frequency sensor for the detection and analysis of aqueous solutions," *IEEE Microw. Wireless Compon. Lett.*, vol. 24, no. 7, pp. 490–492, Jul. 2014.
[9] M. Abdolrazzaghi, S. Khan, and M. Daneshmand, "A dual-mode split-ring resonator to eliminate relative humidity impact," *IEEE Microw. Wireless Compon. Lett.*, vol. 28, no. 10, pp. 939–941, Oct. 2018.
[10] J. Naqui, C. Damm, A. Wiens, R. Jakoby, L. Su, J. Mata-Contreras, and F. Martín, "Transmission lines loaded with pairs of stepped impedance resonators: Modeling and application to differential permittivity measurements," *IEEE Trans. Microw. Theory Techn.*, vol. 64, no. 11, pp. 3864–3877, Nov. 2016.
[11] P. Vélez, K. Grenier, J. Mata-Contreras, D. Dubuc, and F. Martín, "Highly-sensitive microwave sensors based on open complementary split ring resonators (OCSRRs) for dielectric characterization and solute concentration measurement in liquids," *IEEE Access*, vol. 6, pp. 48324–48338, 2018.
[12] M. Abdolrazzaghi, M. Daneshmand, and A. K. Iyer, "Strongly enhanced sensitivity in planar microwave sensors based on metamaterial coupling," *IEEE Trans. Microw. Theory Techn.*, vol. 66, no. 4, pp. 1843–1855, Apr. 2018.
[13] A. Salim and S. Lim, "Complementary split-ring resonator-loaded microfluidic ethanol chemical sensor," *Sensors*, vol. 16, no. 11, p. 1802, Nov. 2016.
[14] P. Vélez, L. Su, K. Grenier, J. Mata-Contreras, D. Dubuc, and F. Martín, "Microwave microfluidic sensor based on a microstrip splitter/combiner configuration and split ring resonators (SRRs) for dielectric characterization of liquids," *IEEE Sensors J.*, vol. 17, no. 20, pp. 6589–6598, Oct. 2017.
[15] L. Su, J. Mata-Contreras, and F. Martín, "Configurations of splitter/combiner microstrip sections loaded with stepped impedance resonators (SIRs) for sensing applications," *Sensors*, vol. 16, no. 12, p. 2195, 2016.
[16] C.-S. Lee and C.-L. Yang, "Single-compound complementary split-ring resonator for simultaneously measuring the permittivity and thickness of dual-layer dielectric materials," *IEEE Trans. Microw. Theory Techn.*, vol. 63, no. 6, pp. 2010–2023, Jun. 2015.
[17] W. Withayachumnankul, K. Jaruwongrungsee, C. Fumeaux, and D. Abbott, "Metamaterial-inspired multichannel thin-film sensor," *IEEE Sensors J.*, vol. 12, no. 5, pp. 1455–1458, May 2012.
[18] T. Chretiennot, D. Dubuc, and K. Grenier, "A microwave and microfluidic planar resonator for efficient and accurate complex permittivity characterization of aqueous solutions," *IEEE Trans. Microw. Theory Techn.*, vol. 61, no. 2, pp. 972–978, Feb. 2013.
[19] A. Ebrahimi, W. Withayachumnankul, S. Al-Sarawi, and D. Abbott, "High-sensitivity metamaterial-inspired sensor for microfluidic dielectric characterization," *IEEE Sensors J.*, vol. 14, no. 5, pp. 1345–1351, May 2014.
[20] L. Su, J. Naqui, J. Mata-Contreras, and F. Martín, "Cascaded splitter/combiner microstrip sections loaded with complementary split ring resonators (CSRRs): Modeling, analysis and applications," in *Proc. IEEE MTT-S Int. Microw. Symp. (IMS)*, May 2016, pp. 1–4.
[21] A. Ebrahimi, J. Scott, and K. Ghorbani, "Differential sensors using microstrip lines loaded with two split-ring resonators," *IEEE Sensors J.*, vol. 18, no. 14, pp. 5786–5793, Jul. 2018.

[22] L. Su, J. Naqui, J. Mata-Contreras, and F. Martín, "Modeling and applications of metamaterial transmission lines loaded with pairs of coupled complementary split-ring resonators (CSRRs)," *IEEE Antennas Wireless Propag. Lett.*, vol. 15, pp. 154–157, 2016.
[23] C. Herrojo, J. Mata-Contreras, F. Paredes, and F. Martín, "Microwave encoders for chipless RFID and angular velocity sensors based on S-shaped split ring resonators," *IEEE Sensors J.*, vol. 17, no. 15, pp. 4805–4813, Aug. 2017.
[24] A. K. Horestani, D. Abbott, and C. Fumeaux, "Rotation sensor based on horn-shaped split ring resonator," *IEEE Sensors J.*, vol. 13, no. 8, pp. 3014–3015, Aug. 2013.
[25] J. Naqui and F. Martín, "Transmission lines loaded with bisymmetric resonators and their application to angular displacement and velocity sensors," *IEEE Trans. Microw. Theory Techn.*, vol. 61, no. 12, pp. 4700–4713, Dec. 2013.
[26] M. S. Boybay and O. M. Ramahi, "Non-destructive thickness measurement using quasi-static resonators," *IEEE Microw. Wireless Compon. Lett.*, vol. 23, no. 4, pp. 217–219, Apr. 2013.
[27] R. Melik, E. Unal, N. K. Perkgoz, C. Puttlitz, and H. V. Demir, "Metamaterial-based wireless strain sensors," *Appl. Phys. Lett.*, vol. 95, no. 1, pp. 011106-1–011106-3, 2009.
[28] W. Su, B. S. Cook, and M. M. Tentzeris, "Additively manufactured microfluidics-based "peel-and-replace" RF sensors for wearable applications," *IEEE Trans. Microw. Theory Techn.*, vol. 64, no. 6, pp. 1928–1936, Jun. 2016.
[29] G. Gennarelli, S. Romeo, M. R. Scarfi, and F. Soldovieri, "A microwave resonant sensor for concentration measurements of liquid solutions," *IEEE Sensors J.*, vol. 13, no. 5, pp. 1857–1864, May 2013.
[30] M. Kirschning, R. H. Jansen, and N. H. L. Koster, "Measurement and computer-aided modeling of microstrip discontinuities by an improved resonator method," in *IEEE MTT-S Int. Microw. Symp. Dig.*, May/Jun. 1983, pp. 495–497.
[31] H.-Y. Yang, N. G. Alexopoulos, and D. R. Jackson, "Microstrip open-end and gap discontinuities in a substrate-superstrate structure," *IEEE Trans. Microw. Theory Techn.*, vol. 37, no. 10, pp. 1542–1546, Oct. 1989.
[32] R. Rodriguez-Berral, F. Mesa, and D. R. Jackson, "Gap discontinuity in microstrip lines: An accurate semianalytical formulation," *IEEE Trans. Microw. Theory Techn.*, vol. 59, no. 6, pp. 1441–1453, Jun. 2011.
[33] K. C. Gupta, *Microstrip Lines and Slotlines* 2nd ed. Boston, MA, USA: Artech House, 1996.
[34] P. Cheong, S.-W. Fok, and K.-W. Tam, "Miniaturized parallel coupled-line bandpass filter with spurious-response suppression," *IEEE Trans. Microw. Theory Techn.*, vol. 53, no. 5, pp. 1810–1816, May 2005.
[35] P. Cheong, K.-F. Chang, W.-W. Choi, and K.-W. Tam, "A highly integrated antenna-triplexer with simultaneous three-port isolations based on multi-mode excitation," *IEEE Trans. Antennas Propag.*, vol. 63, no. 1, pp. 363–368, Jan. 2015.
[36] S.-W. Ting, K.-W. Tam, and R. P. Martins, "Miniaturized microstrip low-pass filter with wide stopband using double equilateral U-shaped defected ground structure," *IEEE Microw. Wireless Compon. Lett.*, vol. 16, no. 5, pp. 240–242, May 2006.
[37] H. Wang, K.-W. Tam, S.-K. Ho, W. Kang, and W. Wu, "Design of ultra-wideband bandpass filters with fixed and reconfigurable notch bands using terminated cross-shaped resonators," *IEEE Trans. Microw. Theory Techn.*, vol. 62, no. 2, pp. 252–265, Feb. 2014.
[38] T. Cheng and K.-W. Tam, "A wideband bandpass filter with reconfigurable bandwidth based on cross-shaped resonator," *IEEE Microw. Wireless Compon. Lett.*, vol. 27, no. 10, pp. 909–911, Oct. 2017.

CHI-HOU CHIO received the B.Sc. degree in electrical and computer engineering from The University of Arizona, Tucson, AZ, USA, in 2009, the M.Sc. degree in electrical and computer engineering from the University of Macau, Macau, China, in 2014, where he is currently pursuing the Ph.D. degree. His research interests include multifunctional microwave circuits and RFID systems.

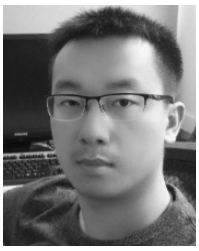

CHENG TENG was born in Hunan, China, in 1991. He received the B.Sc. and M.Sc. degrees in electrical and computer engineering from the University of Macau, Macau, China, in 2013 and 2016, respectively, where he is currently pursuing the Ph.D. degree.

Since November 2013, he has been a Research Assistant with the Wireless Communication Laboratory, Faculty of Science and Technology, University of Macau. His research interests include the UWB bandpass filters, tunable bandpass filters, differential bandpass filters, and RFID systems.

KAM-WENG TAM (S'91–M'01–SM'05) received the B.Sc. degree in electrical and electronics engineering and the joint Ph.D. degree in electrical and electronics engineering from the University of Macau, Macao, China, and the University of Macau and Instituto Superior Técnico (IST), Technical University of Lisbon, Lisbon, Portugal, in 1993 and 2000, respectively.

From 1993 to 1996, he was with the Instituto de Engenharia de Sistemas e Computadores (INESC), Lisbon, Portugal, where he participated in research and development on a broad range of applied microwave technologies for satellite communication systems. From July 2000 to December 2001, he was the Director of the Instituto de Engenharia de Sistemas e Computadores (INESC)–Macau. In 2001, he cofounded the microelectronic design house Chipidea Microelectrónica, Macau, where he was the General Manager, until 2003. Since 1996, he has been with the University of Macau, where he is currently a Professor and the Associate Dean (Research and Graduate Studies) of the Faculty of Science and Technology. He has authored or coauthored over 100 journals and conference papers. His research interests include concerned multifunctional microwave circuits, RFID, UWB for material analysis, and terahertz technology.

Dr. Tam was a member of the organizing committees of 21 international and local conferences, including the Co-Chair of the APMC2008, the Co-Chair of the Technical Program, the IEEE MTT-S International Microwave Workshop Series on Art of Miniaturizing RF and Microwave Passive Components, in 2008, and the Co-Chair of the ISAP2010. He was interim secretary for the establishment of the Macau Section, in 2003. He supervised two IEEE Microwave Theory and Techniques Society (IEEEMTT-S) Undergraduate Scholarship recipients in 2002 and 2003. He was the Founder of the IEEE Macau AP/MTT Joint Chapter, in 2010, and was the Chair, from 2011 to 2012.

WAI-WA CHOI (M'00–SM'10) was born in Macau, China, in 1970. He received the B.Sc., M.Sc., and Ph.D. degrees in electrical and electronics engineering from the University of Macau, Macau, China, in 1993, 1997, and 2008 respectively.

From 1993 to 1995, he was with the Institute of Systems and Computer Engineering (INESC), Lisbon, Portugal, as a Research Assistant. Since 1995, he has been with the University of Macau, where he is currently an Associate Professor with the Department of Electrical and Computer Engineering. He has authored or coauthored over 60 internationally referred journals and conference papers. His research interests include the areas of microwave active and passive circuits, smart antennas, and RF identification (RFID) systems.

Dr. Choi was the Chair of the IEEE Macau Antennas and Propagation/Microwave Theory and Techniques Joint Chapter, in 2015 and 2016.

PEDRO CHEONG (M'15) received the B.Sc., M.Sc., and Ph.D. degrees in electrical and electronics engineering from the University of Macau, Macao, China, in 2000, 2005, and 2014, respectively.

In 2012, he was with the Poly-Grames Research Center, École Polytechnique, University of Montreal, Canada, as a Visiting Researcher, where he is currently with the Wireless Communication Laboratory, as a Laboratory Affair Officer. His research interests include RF/MW passive filter designs, circuit modeling, antenna arrays, RFID systems, multiband communication, and advanced wireless transceiver systems.

Dr. Cheong was the Cofinancial Chair of the 2010 International Symposium on Antennas and Propagation (ISAP). He is the Secretary of the IEEE Macau AP/MTT Joint Chapter, from 2015 to 2017.

SUT-KAM HO was born in Macau, China, in 1974. She received the B.Eng. degree in electrical and electronics engineering from the University of Macau, Macao, China, in 1995, the B.Sc. and M.Phil. degrees in physics from The Hong Kong University of Science and Technology, Hong Kong, in 1997 and 1999, respectively, and the Ph.D. degree in physics from Hong Kong Baptist University, Hong Kong, in 2007. Since 2007, she has been an Assistant Professor with the Faculty of Science and Technology, University of Macau. Her research interests include laser material interaction, spectroscopy, and trace analysis. She pioneered an analytical technique of plume laser-excited atomic fluorescence, which is capable of highly sensitive elemental analysis and successfully applied this tool for the analysis of aqueous and solid samples. Moreover, she used laser spectroscopy to analyze gemstones with minimal destruction of samples and organics thin film with high-resolution depth profiling. She is a member of the Society of Applied Spectroscopy, USA. She is an active member of a few local science promotion programs.